공학석사학위논문

Selective Laser Control of S-bend Shape Memory Alloy Micro Actuator with Metasurface

메타표면을 가지는 S밴드 형상기억합금 마이크로 구동기의 레이저를 이용한 선택적 구동

2019년 8월

서울대학교 대학원

기계항공공학부

이 혜 성

Selective Laser Control of S-bend Shape Memory Alloy Micro Actuator with Metasurface

메타표면을 가지는 S밴드 형상기억합금 마이크로 구동기의 레이저를 이용한 선택적 구동

지도교수 안 성 훈

이 논문을 공학석사 학위논문으로 제출함

2019년 8월

서울대학교 대학원

기계항공공학부

이 혜 성

이혜성의 공학석사 학위논문을 인준함

2019년 8월

위 원 장 _____(인)

부위원장 _____(인)

위 원 _____(인)

Abstract

Selective Laser Control of S-bend Shape Memory Alloy Micro Actuator with Metasurface

Hyesung Lee
Department of Mechanical & Aerospace Engineering
The Graduate School
Seoul National University

Shape Memory Alloys (SMAs) have been widely researched as actuators because SMAs have advantages in high force density and deformable structures. The SMA actuator has a lower actuation speed. To overcome this limit, there have been researched to reduce the size of the actuator to the micro scale in order to use the scale effect of heat transfer. The SMA micro actuator showed higher actuation speed and heat transfer rate than the meso scale actuator. In this research, S-bend shaped actuators were studied to make a

SMA micro actuator. In addition, a metasurface was designed and fabricated on the actuator to enhance the absorption of the laser light at 785 nm wavelength. The metasurface was a lattice array of subwavelength nano cavities, and designed to minimize the reflectance of light at a wavelength of 785 nm. Focused Ion Beam (FIB) was used to fabricate the SMA micro actuator and the metasurface. It was experimentally confirmed that the actuation length of the SMA micro actuator with the metasurface was about twice longer than that without metasurface. It is expected that the absorption spectra of SMA micro actuators can be changed by using the metasurface.

Keyword : Smart material, Shape memory alloy, Metasurface, Focused ion beam machining, Photonic crystal

Student Number : 2017-25695

Contents

Abstract I

Table of Contents III

List of Tables V

List of Figures VI

Table of Contents

Chapter 1. Introduction 1

1.1. Study background 1

1.1.1. Shape memory alloy (SMA) and SMA micro actuator ... 1

1.1.2. Metasurface and light absorber 3

1.1.3. Focused ion beam fabrication 6

1.2. Purpose of research 8

Chapter 2. S-bend SMA micro actuator 9

2.1. Design and Fabrication 9

2.2. Computational Analysis 12

2.3. Evaluation of SMA micro actuators 15

Chapter 3. Metasurface on SMA micro actuator 21

3.1. Machinability of the metasurface 21

3.2. Design of metasurface 23

3.3. Evaluation of the metasurface 28

3.3.1. Fabrication and preparations 28

3.3.2. Results 33

Chapter 4. Conclusion 35

Bibliography 37

Abstract in Korean 41

List of Table

Table 1 Material Properties of SMA (Ni-Ti) 13

Table 2 Designs and parameters of FDTD simulation..... 27

List of Figures

Figure 1 Schematic diagram of SMA crystal structures change [10] 2

Figure 2 Schematic diagram of surface plasmon 5

Figure 3 Light absorbers using plasmonic metamaterials [25, 26] ... 5

Figure 4 Schematic diagram of FIB processes [27] 7

Figure 5 Microscale features fabricated by FIB milling process [28, 29] 7

Figure 6 Image of S-bend shaped SMA micro actuator having 100 degrees of central angle 10

Figure 7 Schematic diagram of the SMA micro actuator fabrication process 11

Figure 8 Computational analysis of S-bend shaped SMA micro actuators 14

Figure 9 Experimental setup for evaluation of the SMA micro actuator 16

Figure 10 Evaluation process of the SMA micro actuator 17

Figure 11 Experimental results of S-bend shaped SMA micro actuators. Central angle were (a) 80 degrees and (b) 100 degrees respectively..... 19

Figure 12 Plot for reaction force versus elongation 20

Figure 13 Machinability test on the surface of SMA 22

Figure 14 Cavity diameter by scan time of the ion beam 22

Figure 15 Reflectance shift in change of periodicities 25

Figure 16 Complex refractive index of Ni-Ti alloy 25

Figure 17 Schematic diagram of the square array of nano cavities and parameters for simulation 26

Figure 18 Reflectance curves of each models from computational analysis results 27

Figure 19 Square array of subwavelength nano cavities fabricated on the SMA micro actuator. (a) Full image of the SMA micro actuator. (b) Array of nano cavities. Radius of each cavity is about 380 nm, and periodicity is 700 nm 29

Figure 20 Experimental setup for actuation test 30

Figure 21 Laser configuration 32

Figure 22 Laser energy versus laser irradiation time 32

Figure 23 Experiment process of the actuation test of the SMA micro actuator with the metasurface 34

Figure 24 Effect of the metasurface on the SMA micro actuator 34

Chapter 1. Introduction

1.1. Study Background

1.1.1. Shape Memory Alloy (SMA) and SMA micro actuator

There has been growing interest in soft actuators using smart materials like shape memory alloys (SMAs), piezoelectric materials, and shape memory polymers [1-5]. Among smart materials, SMAs have the highest value of energy density which makes them useful for application as high force actuators [6-8]. Moreover, SMAs have a specific characteristics such as shape memory effect and superelasticity. Ni-Ti alloy, Nitinol in other words, have outstanding characteristics in the aspect of shape memory effect among other SMAs such as Fe-Mn-Si, Cu-Zn-Al, Cu-Al-Ni alloys [9]. There are two different temperature dependent crystal structures which are called as martensite and austenite respectively. Figure 1 shows the schematic diagram of SMA crystal structures change by two different mechanisms: one is one-way effect, and the other is two-way effect. Under one-way effect, deformation on SMA occurs at its cold state

(austenite). On heating condition, it recovers its original shape, and remain its shape until being deformed again. Under two-way effect, SMA "remembers" two different shapes with specific temperatures. By training the SMA, it is possible to make the SMA to behave in a certain way under specific temperature conditions.

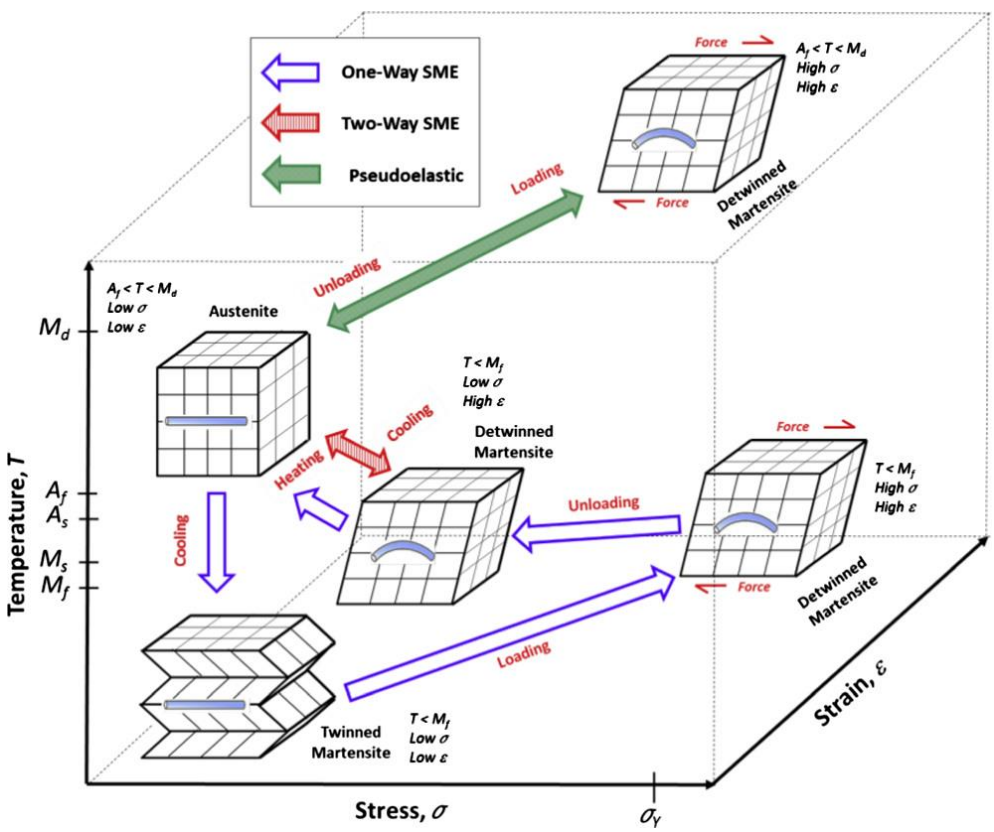

Figure 1 Schematic diagram of SMA crystal structures change [10]

As an actuator, SMAs have high potential of actuation force because of its high force density. The usage of SMA actuators has been enlarged by scaling down the size to micro scale. Under the micro scale, the SMA has high heat convection ratio to the atmospheric material like the air. *Lee et al.* suggested diamond shaped SMA (Ni-Ti alloy) micro actuators with up to 1600Hz actuation speed [11].

1.1.2. Metasurface and light absorber

Metasurface, a 2-D metamaterial, can be used as an array of optical antennas or metallic thin film with dielectric interfaces [12]. The metasurface based on optical antennas changes the behavior of the optical energy which propagates along the surface between the metal and the dielectric material as shown in Figure 2. This characteristics of the metasurface changes transmission, reflection and absorption properties of the material [13-15]. The periodic array of optical antennas makes the incident light to be coupled with electrons on the metallic surface, and it is called surface plasmons (SP) [16]. The excitation of SP modes leads the optical energy at specific wavelength to others such as the heat energy [13]. SP has been used

in sensors [17–19], optical gears like band pass filters or lens [20, 21], and also has been modulated by mechanical deformations [22]. Furthermore, lithography techniques such as ion beam lithography or photolithography have been grown up, so that it is easy to fabricate various type of metasurface and to approach to effective applications [23, 24].

There have been researches to enhance absorption of light by using the mechanism of SP. The light at the specific wavelength is highly absorbed by the metasurface. As shown in Figure 3, *Shi, et al.* suggested the plasmene metasurface absorber which consists of the lattics of Au nano cubes [25]. *Hedayati, et al.* suggested the black absorber using a nearly percolated nano composite [26].

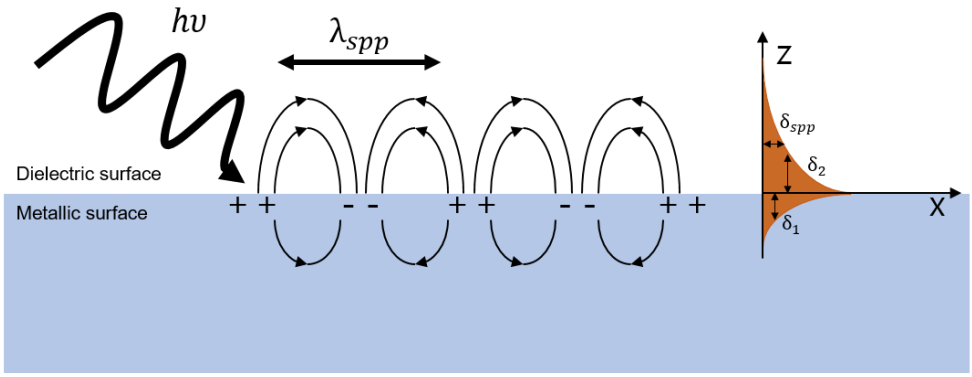

Figure 2 Schematic diagram of surface plasmon [Modified from *Anil Thilsted,* (2013)]

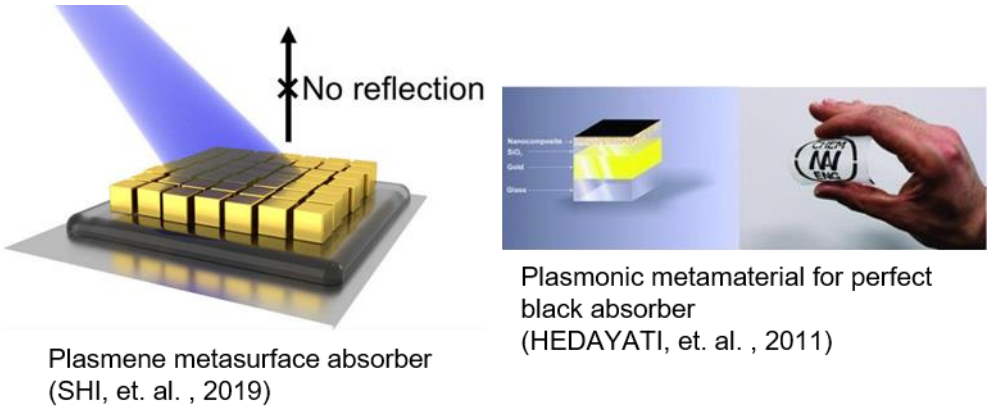

Figure 3 Light absorbers using plasmonic metamaterials [25, 26]

1.1.3. Focused Ion Beam fabrication

Focused Ion Beam (FIB) technique has high advantage in micro- /nano- fabrication process with capability of fine focusing, large energy density, wide choice of ion masses, and short depth of penetration . Moreover, it can directly fabricate the specimen without masking process [27]. Accelerated ions have high potential energy enough to break the surface binding energy of the target, and thus the surface atoms will be sputtered [28, 29]. There are four types in FIB processing, 1) milling, 2) deposition, 3) implantation, 4) imaging [30]. Among these, milling processing is widely used for fabricating the array of nano structures. Figure 5 shows some examples of features made from milling processing [31, 32].

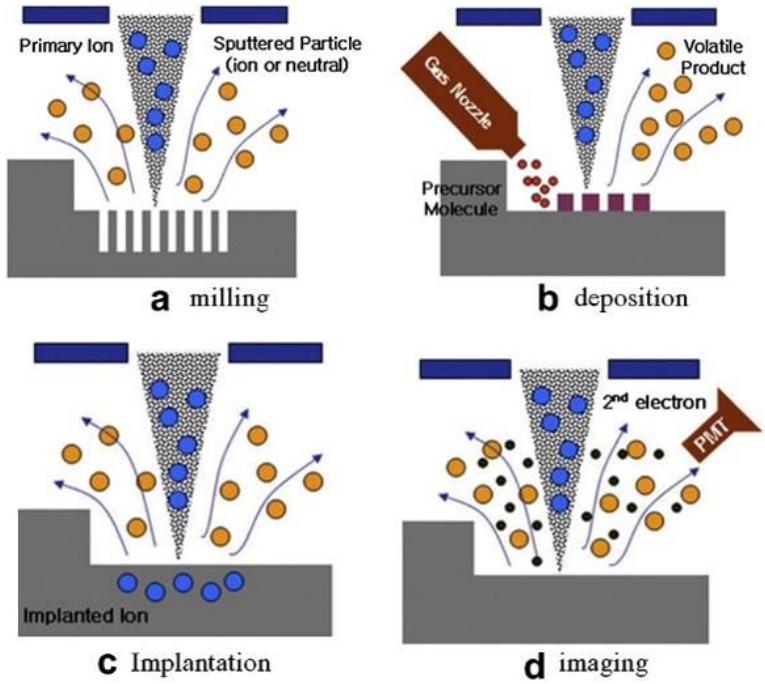

Figure 4 Schematic diagram of FIB processes [30]

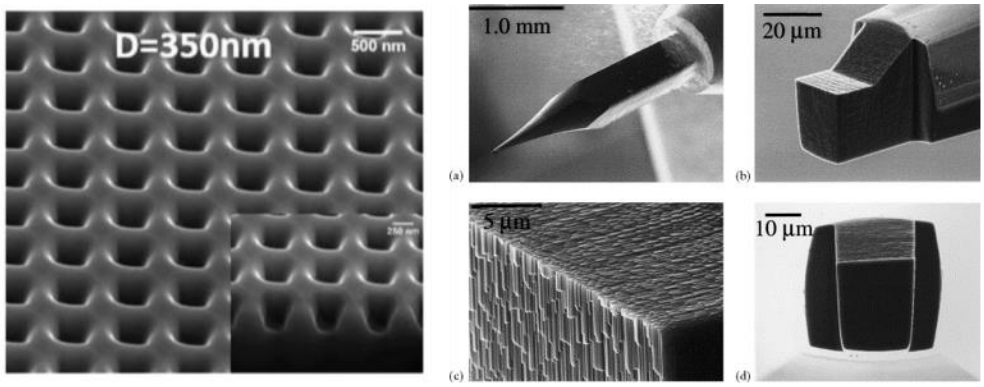

Color filter array fabricated by FIB milling
(GARG et. al. , 2018)

Mechanical cutting tools fabricated by FIB milling process
(Picard, Y.N., et. al. , 2003)

Figure 5 Microscale features fabricated by FIB milling process [31, 32]

1.2. Purpose of Research

Here, we suggest S-bend shaped SMA (Ni-Ti alloy) micro actuators with lattice array of subwavelength nano cavities. S-bend shapes have advantage of avoiding stress concentration under uniaxial tension. As a metasurface, the array of subwavelength nano cavities changed optical spectra of Ni-Ti alloy to achieve enhanced light absorption properties at specific wavelength of light, which does not exist in the nature. This enhancement is expected to enable selective control of the actuation mode for SMA micro actuator with various wavelength of laser lights.

In this research, S-bend SMA micro actuators were fabricated and evaluated with the laser of 355 nm wavelength. The metasurface was designed to enhance absorption of 785 nm wavelength, and fabricated on the actuator. The change of absorption properties by the metasurface was evaluated by suggested actuation test.

Chapter 2. S-bend SMA micro actuator

2.1. Design and Fabrication

To fabricate advanced SMA micro actuator, S-bend shapes were derived and researched. These shapes have no sharpen edge which prevent strain concentration of the structure. As Figure 6 shows, there were three design parameters for this research including central angle, width of the bend and the thickness of the actuator to determine the shape of the S-bend SMA micro actuator. The actuator length is determined by the central angle and the width. Considering the metasurface, thickness and width of the actuator should be large enough to neglect the transmission of the incident light, and maximize the light absorption of the target wavelength. Thus, thickness and width were fixed to 5 and 6 μm respectively for all experiments. The central angles of the arc (edge) were set to 80 and 100 degrees.

Figure 7 shows the schematic diagram of the SMA micro actuator fabrication using FIB milling process to fabricate S-bend SMA micro actuators. First, the SMA wire with diameter of 25 μm was thinned to make flat surface until the desired thickness of the actuator. After thinning process, the thinned wire was rotated for 90 degrees. Then, S-bend shape was fabricated on the flat surface of thinned SMA wire using FIB milling process.

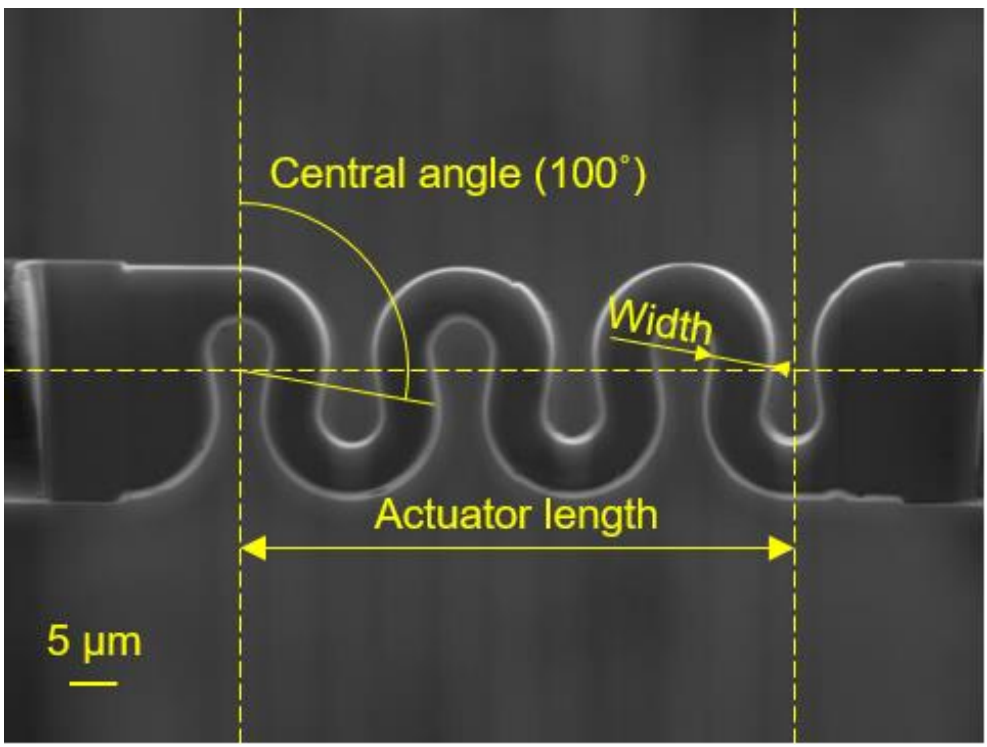

Figure 6 Image of S-bend shaped SMA micro actuator having 100 degrees of central angle

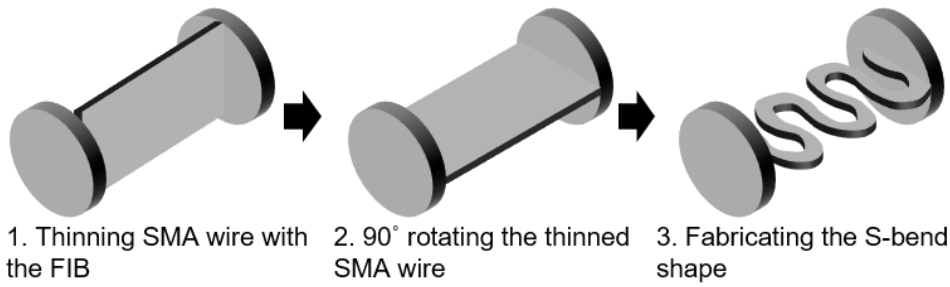

Figure 7 Schematic diagram of the SMA micro actuator fabrication process

2.2. Computational Analysis

It is important to analyze the actuation of fabricated actuator for deeper understanding of actuation mechanism by the geometry of the actuator. Hence, computational analysis was followed using Solidworks (Dassault Systems SolidWorks Corp., France) program. Since the SMA has highly nonlinear characteristics at loading and unloading, nonlinear static analysis was conducted. Table 1 shows mechanical properties of the SMA used in this analysis. The thickness was fixed as 5 μm, and the central angle and the width were controlled independently. The central angles were 85 and 95 degrees, and the widths were 2, 3 and 4 μm, respectively while elongation was fixed as 20 μm. Figure 8 shows the results of reaction forces according to the elongation generated by mechanical loading. The increase of the width of the S-bend occurs the increase of the reaction forces while the central angle does not have significant effect to the reaction forces. Since, the results indicate that it is possible to neglect the central angle as a control variable.

Table 1 Material Properties of SMA (Ni-Ti)

Properties	Value
Elastic Modulus	6×10^{10} N/m^2
Poisson's Ratio	0.3
Initial Yield Stress (Tensile Loading)	6.37×10^{6} N/m^2
Final Yield Stress (Tensile Loading)	9.18×10^{6} N/m^2
Initial Yield Stress (Tensile Unloading)	6.74×10^{6} N/m^2
Final Yield Stress (Tensile Unloading)	2.45×10^{6} N/m^2
Ultimate Plastic Strain Measure (Tension)	0.15
Mass Density	6500 Kg/m^3

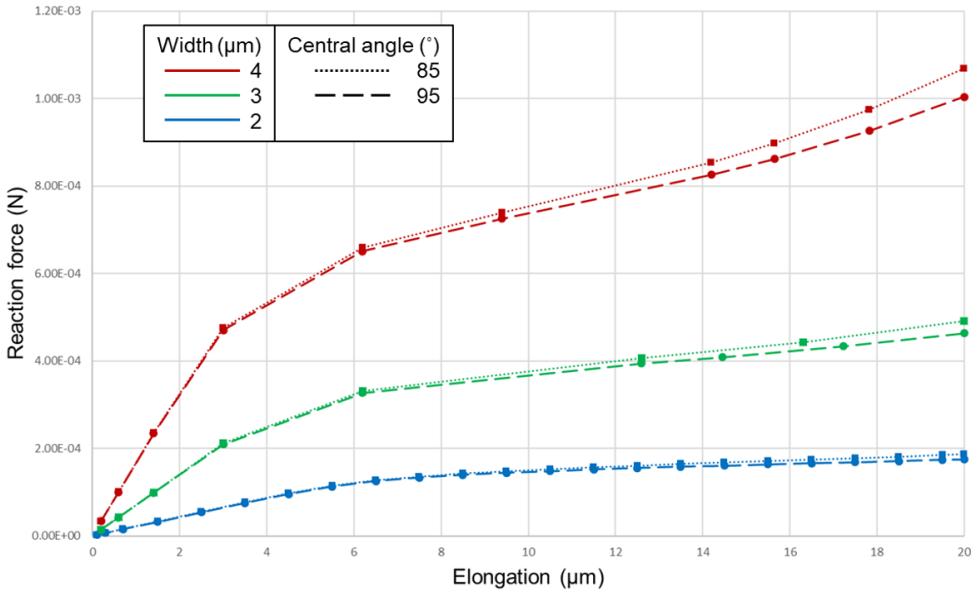

Figure 8 Computational analysis of S-bend shaped SMA micro actuators

2.3. Evaluation of SMA micro actuators

The reaction force was measured during loading and unloading for evaluation of SMA micro actuators. Experimental setup is shown in Figure 9. A 3-axis (X, Y, Z) nano positioner and a microforce sensor end effector (FT-S10000; FemtoTools GmbH, Zurich, Switzerland) were used to load the micro actuator and to measure the reaction force. Both loading and the unloading speeds were 100 nm per second. Samples were held on the plastic fixture with carbon tape. Figure 10 shows the process of the evaluation. First, the sensor was clutched to the end of the actuator. Second, the nano positioner moved and the sensor collected the reaction force. Third, the nano positioner moved in the opposite of loading direction until there was no longer contact between the sensor and the actuator. After that, the sensor was declutched, and the UV laser with 355 nm wavelength (Awave355-4W30K, Advanced Optowave CO., USA) was irradiated to recover the actuator from the martensite state to the austenite state. Finally, previous steps were repeated with gradual increase of elongation until the permanent deformation was occurred.

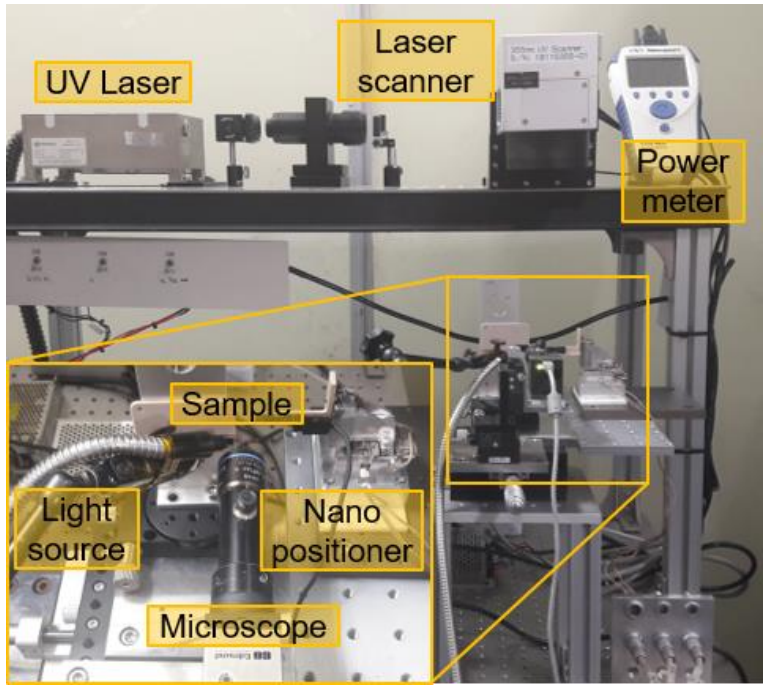

Figure 9 Experimental setup for evaluation of the SMA micro-actuator

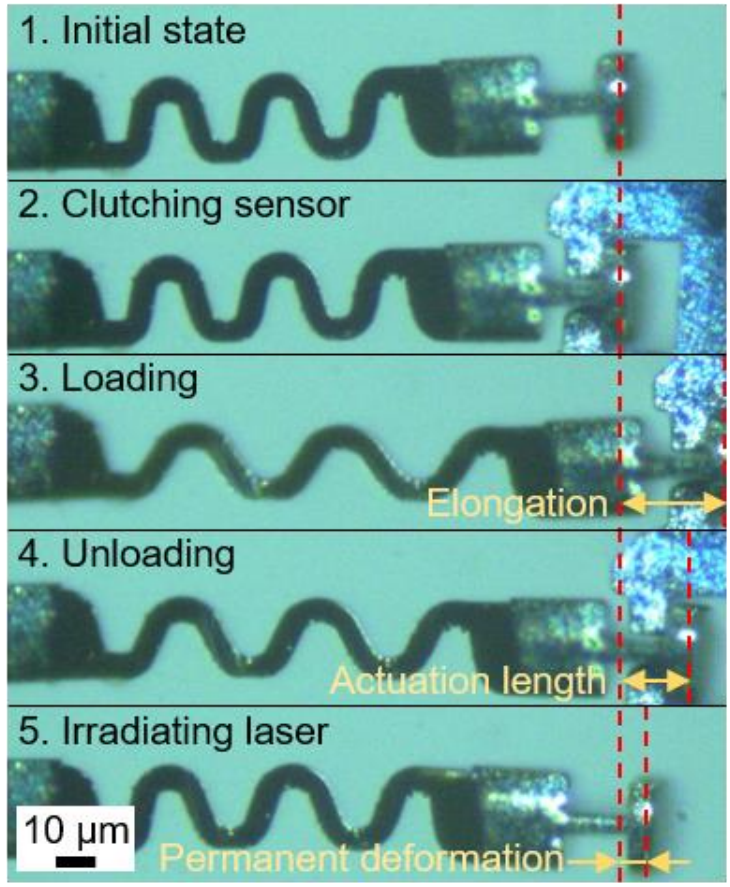

Figure 10 Evaluation process of the SMA micro actuator

Figure 11 and 12 show the results of experiments. In comparison to the computational analysis result (Figure 8) which shows the nonlinearity property of reaction force by the elongation, the reaction force from the experimental result was linearly increased along the elongation. When 20 μm of elongation was loaded, reaction forces of computational analysis and experimental results were nearly the same. (Figure 12) There was no significant difference in actuation performance between each different shapes with equal elongation. It was also confirmed by the computational analysis.

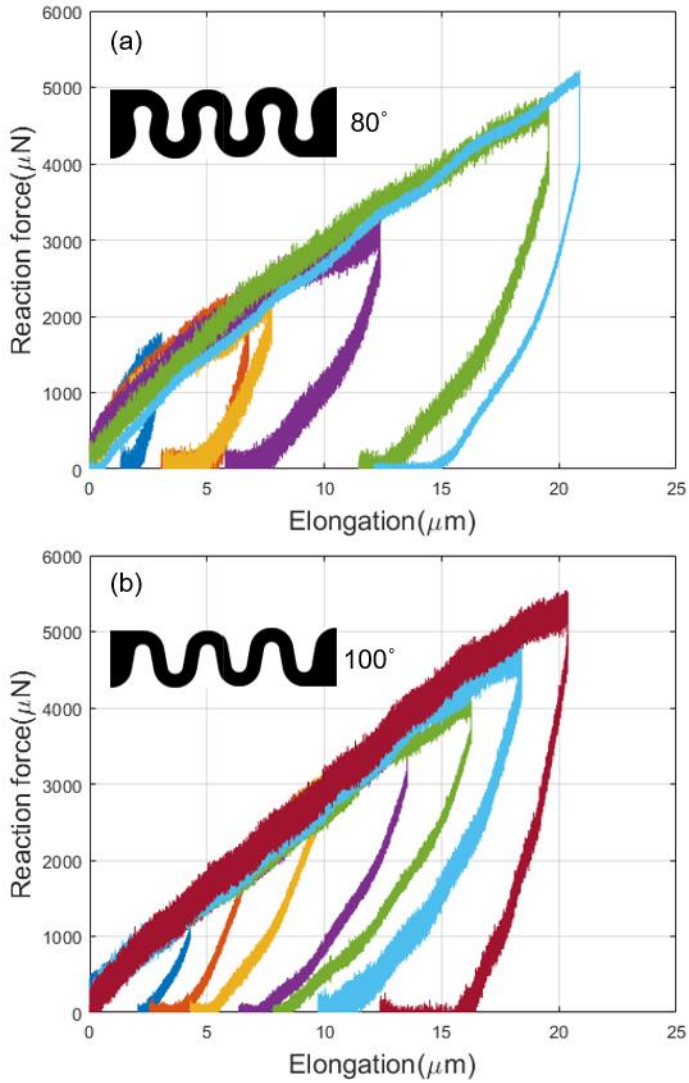

Figure 11 Experimental results of S-bend shaped SMA micro-actuators. Central angle were (a) 80 degrees and (b) 100 degrees respectively

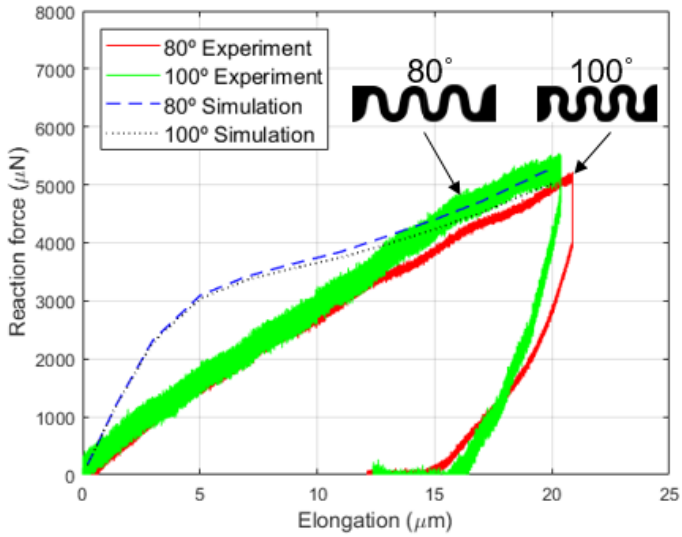

Figure 12 Plot for reaction force versus elongation

Chapter 3. Metasurface on SMA micro actuator

3.1. Machinability of the metasurface

The metasurface was fabricated on SMA micro actuator using FIB milling process. Although the machinability of subwavelength nano patterns on metallic materials including gold, silver, and silicon dioxide was verified in previous studies [13, 33], the machinability on Ni−Ti alloy with equivalent scale have not been verified. Hence, the evaluation of the machinability of a nano cavity on the Ni−Ti alloy was conducted by regulation of parameters of FIB milling process. Ion beam current and beam exposure time (scan time) of FIB were dominant variables that determine features of nano cavities. As a design of experiment, two levels of ion beam current and four levels of scam time were used for this study. Especially, three by three of square arrays with periodicity of 700 nm were fabricated on the thinned SMA wire. There was a linear relationship between the cavity diameter and the scan time with the beam current of 300 pA, while 150 pA does not show significant relationship. Therefore, we chose the beam with the beam current of 300 pA for metasurface fabrication.

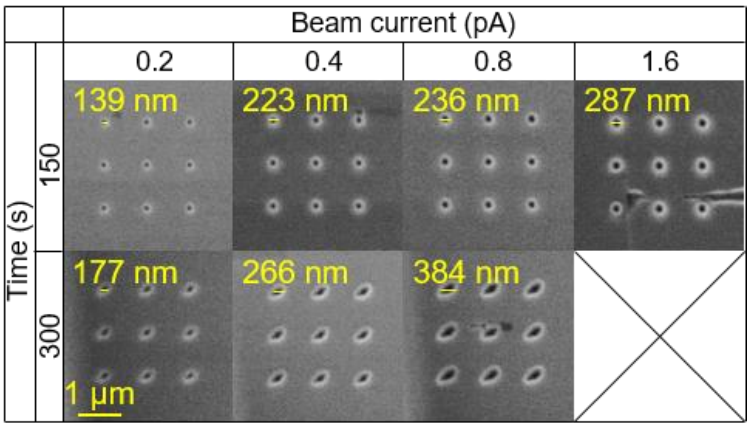

Figure 13 Machinability test on the surface of SMA

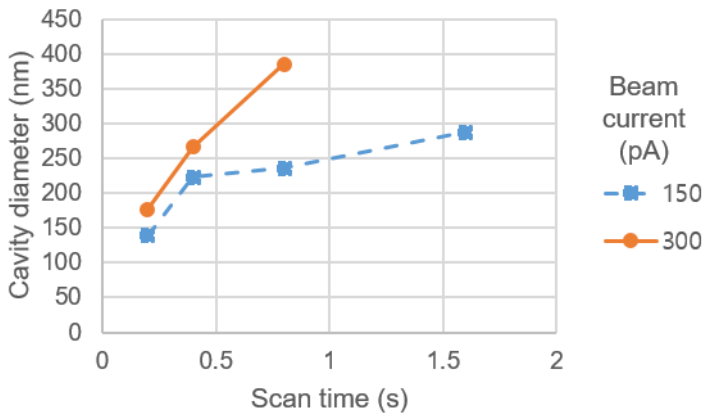

Figure 14 Cavity diameter by scan time of the ion beam

3.2. Design of metasurface

In this research, the metasurface that fabricated on the SMA was designed to decrease the reflectance of the normal incident white light. It is known that an array of subwavelength scale of hole or cavity changes optical properties of metallic materials. As shown in Figure 15, the lowest point of reflectance was dependent to the periodicity. Based on theoretical analysis, it is assumed that scattering of normal incident light is almost neglected in terms of near-field monitoring condition, which means that only reflection and absorption is occurred. Therefore, we designed the subwavelength square array of nano cavity which enhances the absorbance of the light having 785 nm of wavelength. To calculate the optical properties of the square array of nano cavity in theoretical aspect, the finite-difference time-domain (FDTD) method from Lumerical FDTD Solution (Lumerical Inc., Canada) was used. The simulated feature of each nano cavity was designed as a conical shape since it is known that a shape of the nano cavity fabricated by FIB is like a conical shape in previous study. (Figure 5)

To reduce the calculation time, nano cavities were assumed to be arrayed symmetric against 2-D plane (X-Y axis). Figure 17 shows

the scheme of the square array of nano cavities and parameters for simulation. Angle of the incident was set as nominal to the surface with light source of non-polarized plane wave with wavelength range from 0.2 to 1 μm. Ambient environment was set as the air under room temperature (25℃). To acquire optical properties of the metasurface on the SMA (Ni-Ti alloy), it is necessary to input refractive indices and extinction coefficients of the material. However, it is difficult to empirically measure the refractive indices and extinction coefficients of the SMA due to the low machinability of the alloy in several hundreds of micrometer scale precisely. Hence, the optical properties of alloy was estimated according to the previous studies by content ratio of each element constituting the alloy [34, 35]. Especially, the refractive indices and extinction coefficients were calculated in arithmetical mean from each data of Ni and Ti in this study. Figure 16 shows the calculated complex refractive index curve of Ni-Ti. Each data of Ni and Ti were from *Werner et al.* [36]. Based on calculated optical properties and set parameters (Table 2), reflectance curves was calculated as shown in Figure 18. The model 1 was selected to enhance the absorbance of the light having 785 nm wavelength.

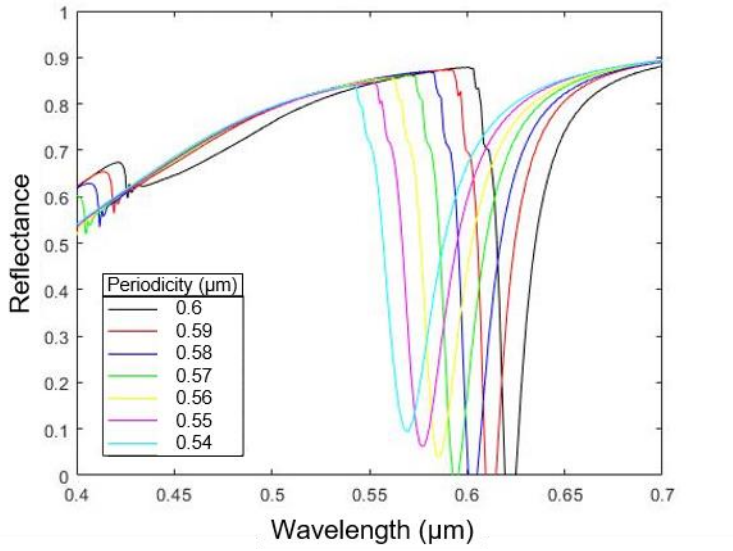

Figure 15 Reflectance shift in change of periodicities

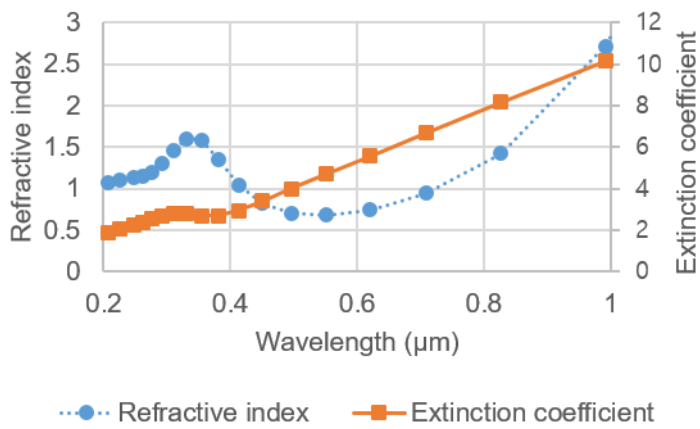

Figure 16 Complex refractive index of Ni−Ti alloy

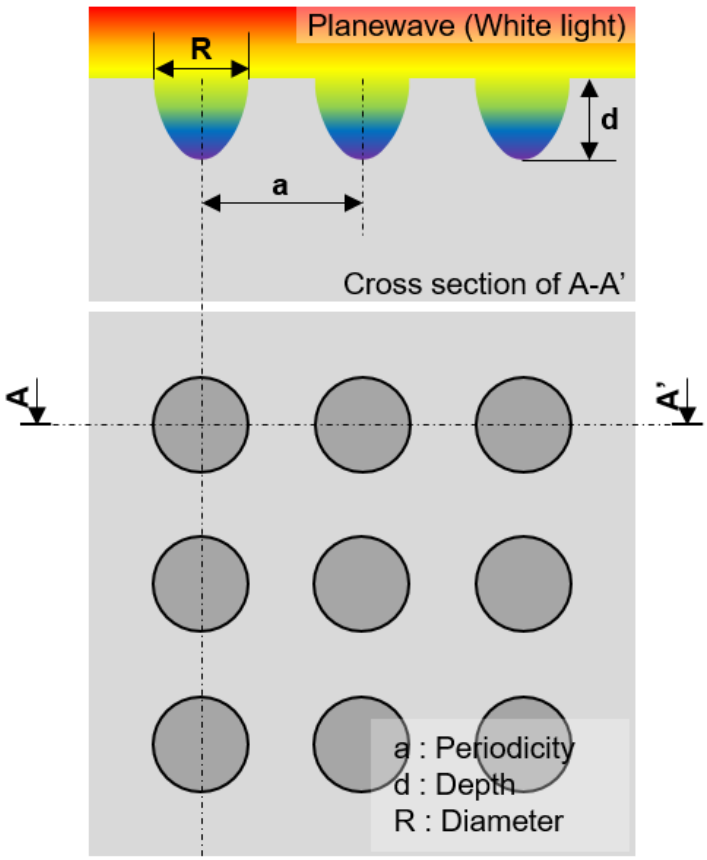

Figure 17 Schematic diagram of the square array of nano cavities and parameters for simulation

Table 2 Designs and parameters of FDTD simulation

	Diameter (R) (nm)	Depth (d) (nm)	Periodicity (a) (nm)
Model 1	380	380	700
Model 2	380	380	750
Model 3	270	300	700
Model 4	270	300	750
Model 5	230	210	600
Model 6	230	210	650

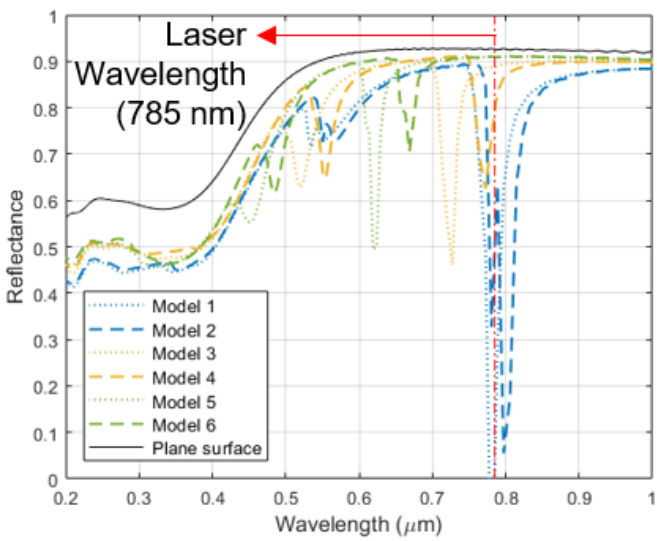

Figure 18 Reflectance curves of each models from computational analysis results

3.3. Evaluation of the metasurface

3.3.1. Fabrication and preparations

According to the hypothesis of this research, it is expected that the metasurface on the SMA occurs the change of absorption rate of the SMA with the laser of specific wavelength, which means that the SMA with the metasurface can be heated by the laser more than that without metasurface. Hence, the actuator with metasurface is expected to have longer actuation length than that without metasurface in terms of the SMA actuators driven by laser heating. To evaluate the effect of metasurface, S-bend shaped SMA micro actuator was first prepared. After that, array of subwavelength nano cavities was fabricated on the actuator by using the FIB (Figure 19). Beam current was 300 pA, and scan time was 0.8 seconds. Experimental setup composed of laser module with output wavelengths of 785 nm is shown in Figure 20. The diode laser (Stradus® 785-80, Vortran Laser Technology, Inc., USA) is used for this study. Spatial mode of the laser was TEM_{00}. M^2 value was under 1.25. Calculated focal spot size of the laser was 71.39 μm. Micro-manager (Vale Lab, UCSF) software was used to control laser

power and irradiation time.

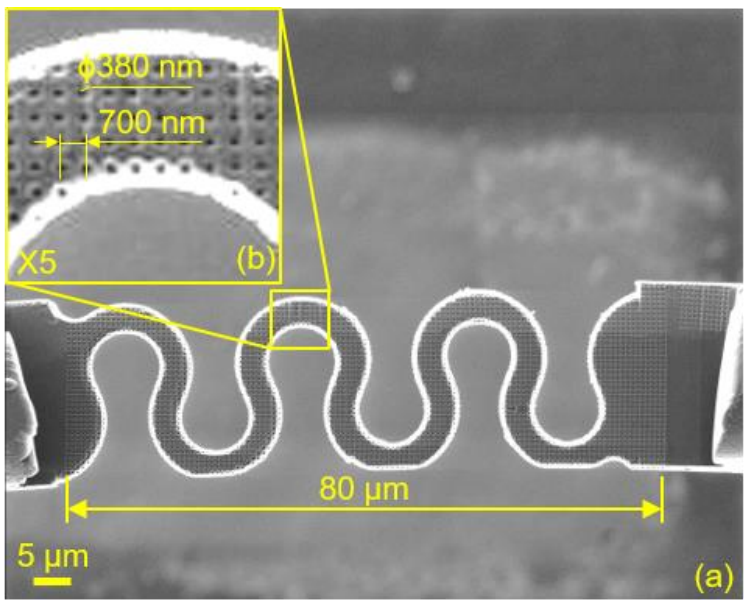

Figure 19 Square array of subwavelength nano cavities fabricated on the SMA micro actuator. (a) Full image of the SMA micro actuator. (b) Array of nano cavities. Radius of each cavity is about 380 nm, and periodicity is 700 nm.

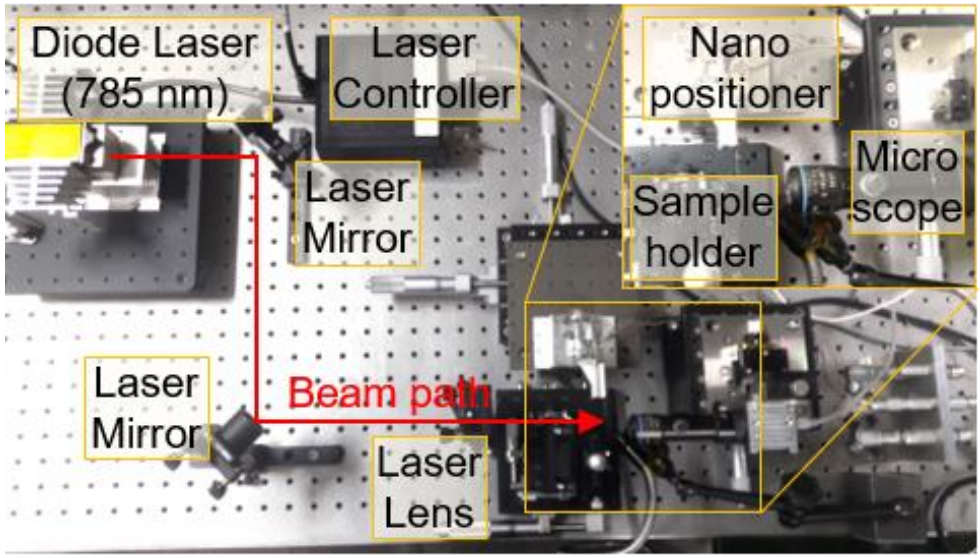

Figure 20 Experimental setup for actuation test.

Before we started the experiment, it was necessary to calculate the laser energy and power versus laser irradiation time because the continuous laser output was controlled to be millisecond pulse laser. Laser power output and shape of the pulse were measured by the powermeter (1919-R, Newport Co, USA). As shown in Figures 21 and 22, measured laser power was converged to its set value as laser irradiation time to be increased. From the result, it was observed that the laser energy exponentially increases by time. The formula for real laser power output is shown as below.

$$E = \frac{P_{set} \cdot (t + a)}{2(1 - e^{c(t+a)})}$$

where

$E = Laser\ \ energy\ \ (\mu J)$

$P_{set} = Set\ \ laser\ \ power\ \ output\ \ (mW)$

$t = set\ \ irradiation\ \ time\ \ (ms)$

$a = time\ \ offset\ \ (ms)$

$c = -0.00145\ \ (const)$

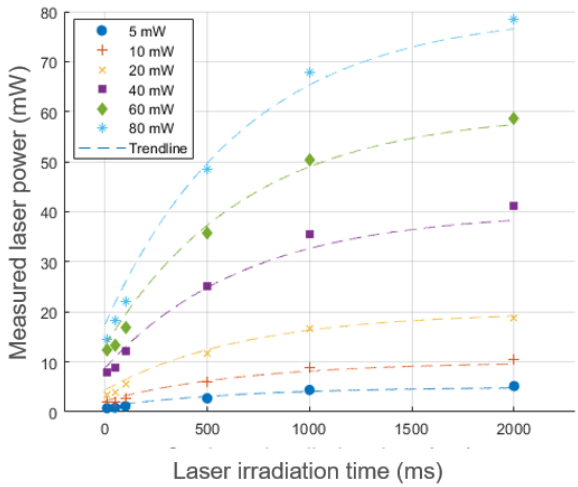

Figure 21 Laser configuration

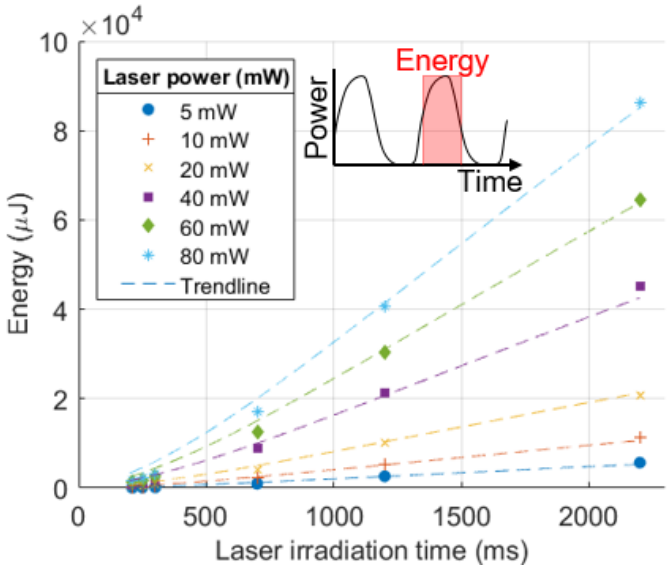

Figure 22 Laser energy versus laser irradiation time

3.3.2. Results

In the experiment, laser irradiation time was fixed to 500 ms. Stretched length of the micro actuator was fixed to 10 μm. A 3-axis (X, Y, Z) nano positioner and micro grippers (SG-1730, Smaract GmbH, Germany) were used to load the micro actuator. After unloading, elongation of the micro actuator was about 4.9 μm. Figure 23 shows experimental process. The micro actuator was stretched by using the micro gripper. After stretching, the micro gripper left the micro actuator, and the spring back of micro actuator occurred. Finally, the laser light was irradiated to actuate. Figure 24 shows the difference of the actuation length between the specimen with the metasurface and that without the metasurface. After heating with the laser, Actuation length of the specimen with the metasurface was about 223% longer than that without the metasurface under 20 mW of laser power condition. Results of the specimen with metasurface converge to its maximum restored ratio after 20 mW of laser power irradiation. Also, the restored length and the laser power are linear to each other until it reaches to maximum.

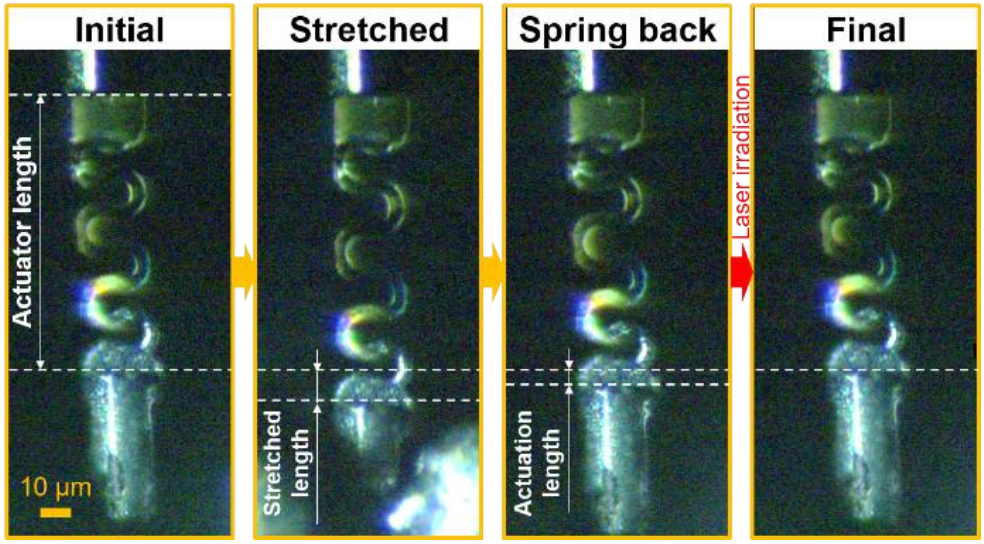

Figure 23 Experiment process of the actuation test of the SMA micro actuator with the metasurface

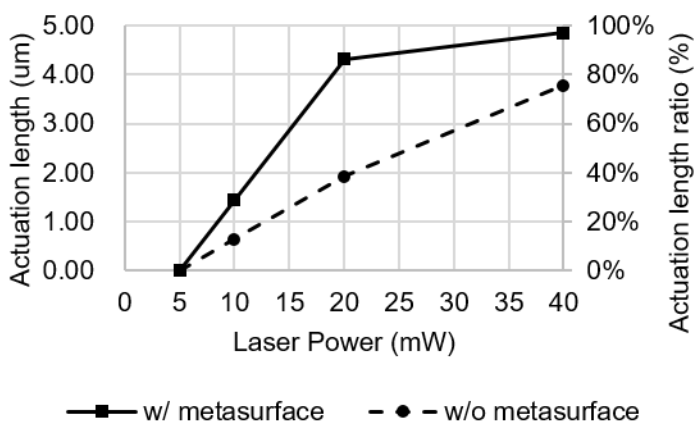

Figure 24 Effect of the metasurface on the SMA micro actuator

Chapter 4. Conclusion

In this study, S-bend SMA micro actuator with metasurface was designed and fabricated to achieve selective laser control driven by laser heating with various wavelength. First, S-bend shape memory alloy actuators were designed and fabricated using FIB milling process which has its advantages of micro/nano fabrication process. The computational analysis was conducted to evaluate the significance of design parameters of S-bend shape memory alloy actuator including the width and the central angle.

Second, the metasurface was designed, and fabricated on S-bend shape memory alloy using also FIB milling process. To evaluate the machinability of SMA in FIB milling process, process parameterization for the beam current and scan time was conducted. The metasurface was designed from the machinability data of nano cavities using FIB milling process, and analyzed using FDTD method. Hence, the lattice array of nano cavities with unit diameter of 380 nm and periodicity of 700 nm was designed to decrease the reflectance of the light with 785 nm wavelength.

Finally, evaluation of the SMA micro actuator with the metasurface

was conducted by the laser light at 785 nm wavelength. The experimental results show that the actuation length of the SMA micro actuator with the metasurface was about 223% longer than that without the metasurface under 20 mW of laser power condition. From the results of this research, it is expected to promise new ways for the development of multi-mode control micro robots.

Bibliography

[1] M. Zarek, M. Layani, I. Cooperstein, E. Sachyani, D. Cohn, and S. Magdassi, "3D printing of shape memory polymers for flexible electronic devices," *Advanced Materials,* vol. 28, no. 22, pp. 4449–4454, 2016.

[2] H. Rodrigue, W. Wang, D.–R. Kim, and S.–H. Ahn, "Curved shape memory alloy–based soft actuators and application to soft gripper," *Composite Structures,* vol. 176, pp. 398–406, 2017.

[3] J. Liu, Y. Liu, L. Zhao, D. Xu, W. Chen, and J. Deng, "Design and experiments of a single–foot linear piezoelectric actuator operated in a stepping mode," *IEEE Transactions on Industrial Electronics,* vol. 65, no. 10, pp. 8063–8071, 2018.

[4] H. Rodrigue, W. Wang, M.–W. Han, T. J. Kim, and S.–H. Ahn, "An overview of shape memory alloy–coupled actuators and robots," *Soft Robotics,* vol. 4, no. 1, pp. 3–15, 2017.

[5] A. Miriyev, K. Stack, and H. Lipson, "Soft material for soft actuators," *Nature Communications,* vol. 8, no. 1, p. 596, 2017.

[6] J. J. Song, H. H. Chang, and H. E. Naguib, "Biocompatible shape memory polymer actuators with high force capabilities," *European Polymer Journal,* vol. 67, pp. 186–198, 2015.

[7] K. Andrianesis and A. Tzes, "Development and control of a multifunctional prosthetic hand with shape memory alloy actuators," *Journal of Intelligent & Robotic Systems,* vol. 78, no. 2, pp. 257–289, 2015.

[8] W. Wang and S.–H. Ahn, "Shape memory alloy–based soft gripper with variable stiffness for compliant and effective grasping," *Soft Robotics,* vol. 4, no. 4, pp. 379–389, 2017.

[9] N. Choudhary and D. Kaur, "Shape memory alloy thin films and heterostructures for MEMS applications: a review," *Sensors and Actuators A: Physical,* vol. 242, pp. 162–181, 2016.

[10] J. M. Jani, M. Leary, A. Subic, and M. A. Gibson, "A review of shape memory alloy research, applications and opportunities," *Materials & Design (1980–2015),* vol. 56, pp. 1078–1113, 2014.

[11] H. T. Lee, M. S. Kim, G. Y. Lee, C. S. Kim, and S. H. Ahn, "Shape Memory Alloy (SMA)-Based Microscale Actuators

with 60% Deformation Rate and 1.6 kHz Actuation Speed," *Small,* vol. 14, no. 23, pp. 1801023, 2018.
[12] N. Yu and F. Capasso, "Flat optics with designer metasurfaces," *Nature Materials,* vol. 13, no. 2, pp. 139, 2014.
[13] A. G. Brolo, E. Arctander, R. Gordon, B. Leathem, and K. L. Kavanagh, "Nanohole-enhanced Raman scattering," *Nano Letters,* vol. 4, no. 10, pp. 2015-2018, 2004.
[14] W. L. Barnes, A. Dereux, and T. W. Ebbesen, "Surface plasmon subwavelength optics," *Nature,* vol. 424, no. 6950, pp. 824, 2003.
[15] Y. Fleger and M. Rosenbluh, "Surface plasmons and surface enhanced Raman spectra of aggregated and alloyed gold-silver nanoparticles," *International Journal of Optics,* vol. 2009, 2009.
[16] H.-T. Chen, A. J. Taylor, and N. Yu, "A review of metasurfaces: physics and applications," *Reports on Progress in Physics,* vol. 79, no. 7, pp. 076401, 2016.
[17] L. Cong, S. Tan, R. Yahiaoui, F. Yan, W. Zhang, and R. Singh, "Experimental demonstration of ultrasensitive sensing with terahertz metamaterial absorbers: A comparison with the metasurfaces," *Applied Physics Letters,* vol. 106, no. 3, pp. 031107, 2015.
[18] Y. Lee, S.-J. Kim, H. Park, and B. Lee, "Metamaterials and metasurfaces for sensor applications," *Sensors,* vol. 17, no. 8, pp. 1726, 2017.
[19] A. Dhawan, M. Canva, and T. Vo-Dinh, "Narrow groove plasmonic nano-gratings for surface plasmon resonance sensing," *Optics Express,* vol. 19, no. 2, pp. 787-813, 2011.
[20] Q. Wang *et al.*, "A broadband metasurface-based terahertz flat-lens array," *Advanced Optical Materials,* vol. 3, no. 6, pp. 779-785, 2015.
[21] Y. Lee *et al.*, "Electrical broad tuning of plasmonic color filter employing an asymmetric-lattice nanohole array of metasurface controlled by polarization rotator," *ACS Photonics,* vol. 4, no. 8, pp. 1954-1966, 2017.
[22] J. Valente, E. Plum, I. J. Youngs, and N. I. Zheludev, "Nano-and Micro-Auxetic Plasmonic Materials," *Advanced Materials,* vol. 28, no. 26, pp. 5176-5180, 2016.
[23] G. Yoon, I. Kim, and J. Rho, "Challenges in fabrication towards realization of practical metamaterials," *Microelectronic*

Engineering, vol. 163, pp. 7–20, 2016.
[24] M. Nasr *et al.*, "Narrowband metamaterial absorber for terahertz secure labeling," *Journal of Infrared, Millimeter, and Terahertz Waves,* vol. 38, no. 9, pp. 1120–1129, 2017.
[25] Q. Shi *et al.*, "Plasmene Metasurface Absorbers: Electromagnetic Hot Spots and Hot Carriers," *ACS Photonics,* vol. 6, no. 2, pp. 314–321, 2019.
[26] M. K. Hedayati *et al.*, "Design of a perfect black absorber at visible frequencies using plasmonic metamaterials," *Advanced Materials,* vol. 23, no. 45, pp. 5410–5414, 2011.
[27] J. J. Wang, X. Chang, and X. F. Zong, "Focused ion beam analysis technology," in *1998 5th International Conference on Solid–State and Integrated Circuit Technology. Proceedings (Cat. No. 98EX105)*, 1998, pp. 311–314: IEEE.
[28] A. Dubner, A. Wagner, J. Melngailis, and C. Thompson, "The role of the ion-solid interaction in ion-beam-induced deposition of gold," *Journal of Applied Physics,* vol. 70, no. 2, pp. 665–673, 1991.
[29] R. Behrisch and W. Eckstein, "Sputtering yield increase with target temperature for Ag," *Nuclear Instruments and Methods in Physics Research Section B: Beam Interactions with Materials and Atoms,* vol. 82, no. 2, pp. 255–258, 1993.
[30] C.–S. Kim, S.–H. Ahn, and D.–Y. Jang, "Developments in micro/nanoscale fabrication by focused ion beams," *Vacuum,* vol. 86, no. 8, pp. 1014–1035, 2012.
[31] V. Garg, R. G. Mote, and J. Fu, "Focused Ion Beam Direct Fabrication of Subwavelength Nanostructures on Silicon for Multicolor Generation," *Advanced Materials Technologies,* vol. 3, no. 8, pp. 1800100, 2018.
[32] Y. N. Picard, D. Adams, M. Vasile, and M. Ritchey, "Focused ion beam–shaped microtools for ultra–precision machining of cylindrical components," *Precision Engineering,* vol. 27, no. 1, pp. 59–69, 2003.
[33] G. Biener, A. Niv, V. Kleiner, and E. Hasman, "Metallic subwavelength structures for a broadband infrared absorption control," *Optics Letters,* vol. 32, no. 8, pp. 994–996, 2007.
[34] G. Laws, E. Larkins, I. Harrison, C. Molloy, and D. Somerford, "Improved refractive index formulas for the Al x Ga 1− x N and In y Ga 1− y N alloys," *Journal of Applied Physics,* vol. 89, no. 2, pp. 1108–1115, 2001.

[35] C. Teng *et al.*, "Refractive indices and absorption coefficients of Mg x Zn 1− x O alloys," *Applied Physics Letters,* vol. 76, no. 8, pp. 979−981, 2000.
[36] W. S. Werner, K. Glantschnig, and C. Ambrosch−Draxl, "Optical constants and inelastic electron−scattering data for 17 elemental metals," *Journal of Physical and Chemical Reference Data,* vol. 38, no. 4, pp. 1013−1092, 2009.

요약(국문초록)

형상기억합금(Shape Memory Alloy, SMA)는 높은 힘 밀도와 변형 가능한 구조를 가지는 장점 덕분에 구동기로서 연구되어왔다. 형상기억합금 구동기는 구동력에 비해 낮은 구동속도를 가지고 있어, 이를 극복하기 위해 크기 효과 (Size effect)를 이용하고자 구동기의 크기를 마이크로 수준으로 낮추는 연구가 진행되어왔다. 이렇게 연구된 형상기억합금 마이크로 구동기는 메소스케일 구동기와 비교하면 보다 높은 구동 속도, 변형률, 열 전달률을 가진다. 전기저항으로 온도를 제어하는 대신 마이크로 스케일에서는 자외선 파장의 레이저로 구동되는 특징을 보인다. S밴드 형상을 가지는 마이크로 구동기를 제안하였고, 구동원을 가시광선 및 적외선 영역으로 확장하고자 메타표면(Metasurface)을 구동기 표면에 제작하였다. 메타표면은 파장 이하 길이를 가지는 나노 홈 격자 구조로 이루어져 있으며, 785 nm 파장의 빛의 반사율을 최소화하는 방향으로 설계되었다. 형상기억합금 마이크로 구동기 및 메타표면을 제작하기 위해 집속이온빔(Focused Ion Beam, FIB)이 사용되었다. 결과적으로, 785 nm 파장의 구동원에서 메타표면을 가지는 형상기억합금 마이크로 구동기의 구동 길이가 메타표면을 가지지 않는 구동기보다 약 223% 더 긴 것을 실험적으로 확인하였다. 본 연구를 통해 형상기억합금 마이크로 구동기의 구동원을 확장할 수 있고, 구동원에 따라 선택적으로 구동을 할 수 있을 것으로 기대한다.

주요어 : 지능재료, 형상기억합금, 집속이온빔, 메타표면, 광결정

학번: 2017-25695